University of Arkansas, Fayetteville
ScholarWorks@UARK

Physics Undergraduate Honors Theses | Physics

5-2023

Fabrication of Black Phosphorus Terahertz Photoconductive Antennas

Nathan Tanner Sawyers
University of Arkansas, Fayetteville

Follow this and additional works at: https://scholarworks.uark.edu/physuht

 Part of the Condensed Matter Physics Commons, Electronic Devices and Semiconductor Manufacturing Commons, Nanotechnology Fabrication Commons, and the Semiconductor and Optical Materials Commons

Citation

Sawyers, N. T. (2023). Fabrication of Black Phosphorus Terahertz Photoconductive Antennas. *Physics Undergraduate Honors Theses* Retrieved from https://scholarworks.uark.edu/physuht/16

This Thesis is brought to you for free and open access by the Physics at ScholarWorks@UARK. It has been accepted for inclusion in Physics Undergraduate Honors Theses by an authorized administrator of ScholarWorks@UARK. For more information, please contact scholar@uark.edu, uarepos@uark.edu.

Fabrication of Black Phosphorus Terahertz Photoconductive Antennas

An Honors Thesis submitted in partial fulfillment of the requirements of

Honors Studies in Physics

By

Nathan Tanner Sawyers

Spring 2023

Physics

Fulbright College of Arts and Sciences

The University of Arkansas

Acknowledgements

I would like to thank Dr. Hugh Churchill and the University of Arkansas for giving me a fruitful undergraduate research experience. I would also like to thank Katie Welch for her endless guidance, instruction, and advice on lab equipment and the fabrication process.

Table of Contents

Abstract

Terahertz (THz) photoconductive antennas (PCAs) using 40nm thin-film flakes of black phosphorus (BP) and hexagonal boron nitride (hBN) have been shown computationally to be capable of THz emission comparable to those based on GaAs [2]. In this paper, I briefly describe the scientific and practical interest in THz emissions and explain what warrants research into black phosphorus as a photoconductive semiconductor in THz devices. Furthermore, I outline the basic principle of how these antennas work and mention alternative designs produced by other researchers in the past. Finally, I summarize the fabrication process of these antennas, as well as the measurements of an antenna produced by myself and graduate student Katie Welch.

Background

The shift toward wireless devices and communication necessitates the development of electromagnetic technology that can support greater amounts of data traffic [3]. Terahertz (THz) waves, which lie between microwave and infrared waves on the electromagnetic spectrum, offer a medium through which data transfer rates could reach gigabit-per-second or even terabit-per-second speeds using polarization multiplexing [3][5]. THz waves also offer a number of superior properties that other frequencies do not, such as low risk of biological harm and high spectral resolution [3]. Other applications of THz radiation have been proposed, including THz imaging and spectroscopy [1]. However, THz waves – unlike microwave or infrared waves – have not seen widespread use due to the lack of technology capable of producing and detecting them [5]. The development of THz antennas may challenge that.

In the past two decades, THz antennas, which are used to produce and detect terahertz-frequency electromagnetic radiation, have been manufactured with a variety in design.

In particular, proposed and realized THz antennas include metallic horn antennas, dielectric substrate antennas, and “new material” antennas, such as Samir Mahmoud and Ayed AlAjmi’s carbon nanotube configuration [3][4]. However, in recent years the field of photoconductive antennas (PCAs) has gained interest. In principle, these devices use a photoconductive semiconductor, such as GaAs [1], to generate broadband THz pulses when excited by a laser pulse [2]. This excitation creates an electron-hole pair in the semiconductor which allows for current to flow when a voltage bias is present. With a short enough laser pulse (typically around 100fs), this current will produce THz radiation from the antenna [3].

Although this has been successful with low-temperature-grown GaAs, that material has low power conversion efficiency from laser to signal, and devices using it would require other approaches to boost this conversion efficiency [2]. One alternative is to use 2-dimensional black phosphorus as the semiconductor instead of GaAs. BP is a material with an anisotropic crystal structure with a high saturation velocity and strong absorption in the “armchair” direction (as opposed to the “zig-zag” direction). Furthermore, 2D BP has a low electron density (measured as low as 6.5e11 cm^{-2}) and high room-temperature carrier mobility (measured as high as 1615cm^2/Vs)[7]. However, BP is oxygen-sensitive and must be handled only in an oxygen-free glovebox. To shield the flake of BP from oxygen, we use a wider, thin layer of hexagonal boron nitride.

Methods

A. Exfoliation and Flake Analysis

In order to obtain ideal BP and hBN flakes, we use a process called mechanical exfoliation. In this process, thin layers are peeled off of bulk crystals using adhesive tape. Resulting flakes are placed onto silicon substrate chips, which are then cleaned with isopropyl

alcohol and acetone to remove glue residue from the chips. It has been demonstrated by Josh Thompson [6] that heating the tape and substrate while in contact leads to larger BP flake yield, and this indeed matches our observations. During exfoliation, we heated each BP-covered tape strip and substrate to 100°C for two minutes and then allowed it to cool to room temperature before peeling. This process results in a wide variety of flake thickness and uniformity.

Figure 1:
Two candidate flakes, BP (left) and hBN (right) are identified by their color, size, and uniformity.

In this device, BP flakes around 40nm thick and hBN flakes around 10nm thick are ideal [2], and these flakes are located on the substrate using a standard 20x optical microscope, as shown in figure 1. In order for an ideal BP flake to span the dipole gap of an antenna, it needs to be at least 8µm by 8µm square, and hBN should be at least 20µm by 20µm in order to fully cover the corresponding BP flake. Approximate size can be easily measured using the optical microscope (see figure 2), and flake thickness can be approximated by the color of the flake. On the microscope in the Churchill Lab, 40nm-thick black phosphorus typically appears a golden yellow color, as shown

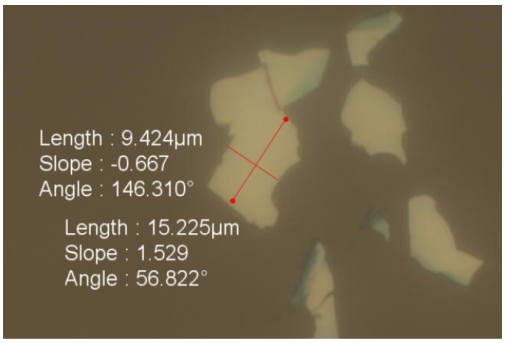

Figure 2:
A satisfactory section of BP is measured to be approximately 9µm by 15µm. It appears uniform, and its color suggests ideal thickness.

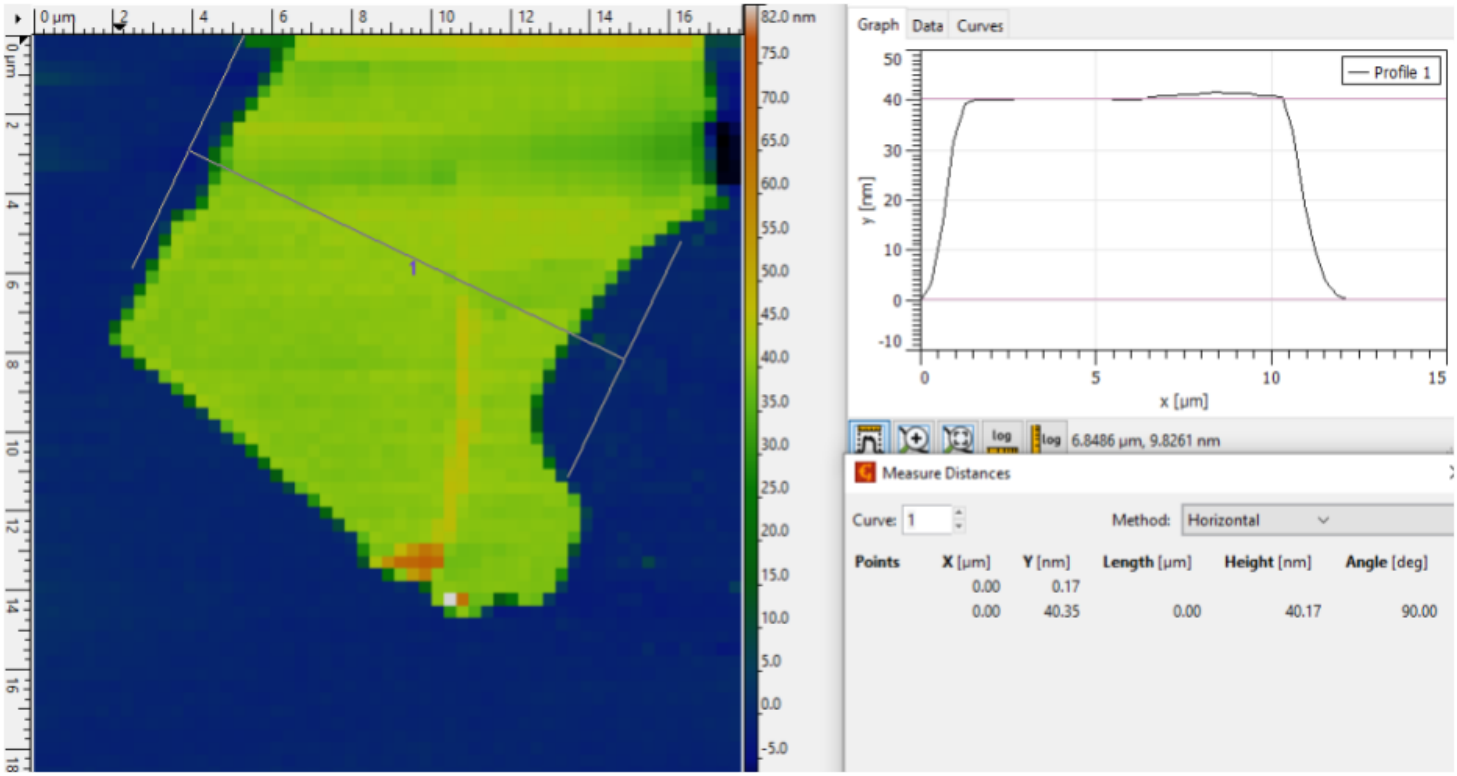

Figure 3:
The thickness ("height") of a black phosphorus flake is measured along a cross-section of the flake and graphed. This image and graph confirm the uniformity of the flake and measure its thickness to be approximately 40nm thick.

in figure 2. In order to verify these dimensions, the use of an atomic force microscope (AFM) was used. This device is able to accurately image the topography of BP and hBN flakes, ensuring that every used flake is uniform and lacks holes, folds, and impurities that may expose the BP flake to oxygen, short-circuit the antenna, create an abnormality in the crystal's lattice structure, or otherwise introduce error to the experiment. An AFM-produced graph corresponding to the thickness of a flake is shown in figure 3. Since operating the AFM typically requires a few hours of dedicated time for locating, positioning, and scanning, it is beneficial to only measure flakes that appear to be of (or near) the right size and thickness.

Unlike some other photoconductive semiconductors, BP has an anisotropic lattice structure, resulting in different optical and electrical constants along the armchair and zigzag

directions [2]. We determine the orientation of the crystal axis through differential reflectance anisotropy, also known as reflectance anisotropy spectroscopy. In this process, polarized monochromatic light with a wavelength $\lambda = 650nm$ is split, with one part exciting the BP flake and reflecting back and the other part left alone. By comparing the intensity of these two paths of light, we can measure the reflectance and thus absorption of the crystal. By changing the polarization direction, we can deduce which orientation would maximize absorption, in this case the armchair axis. For this fabrication, we made two measurements each on the BP flake and substrate, and then changed the polarization angle and once again measured on the BP flake and substrate. The measurements on the substrate are used to verify the laser and setup are functional and consistent, as well as normalize the data produced by the BP flake trials. The normalized results of measuring one particular flake can be seen in figure 4.

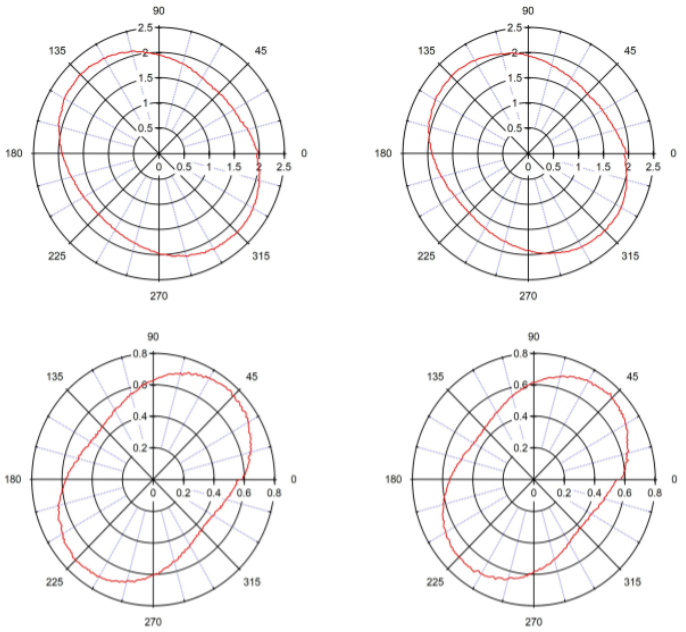

Figure 4:
Anisotropy measurements of the BP flake create polar graphs identifying the orientation of the crystal structure in the flake.

Exfoliation and AFM measurements can easily be done in a glovebox, however, the fabrication process involves the use of in-air measurements, namely the anisotropy measurement described above. To remedy this, we use hermetic transfer cells developed by Josh Thompson [6], which have a glass microscope slide to see and analyze the samples within. These cells ease the process of optically searching for flakes and expedite the fabrication process. However, it

should be noted that these transfer cells can fail or crack, so if possible, leaving these cells outside of a glovebox for prolonged periods should be avoided.

B. Antenna Fabrication

In order to create the antenna itself, we use a technique called electron beam lithography. This involves adding a thin resist layer to a clean wafer, and then using a beam of electrons to carve out the desired pattern in the resist layer. By exposing this pattern to a solution of hydrofluoric acid, we can carve or etch the pattern into the wafer itself. Metal – in this case gold – is evaporated, and it condenses in the etched pattern as well as on the resist. After removing the resist layer, all that remains is the substrate with an engraved gold pattern, which forms the electrodes of the antenna as shown in figure 6.

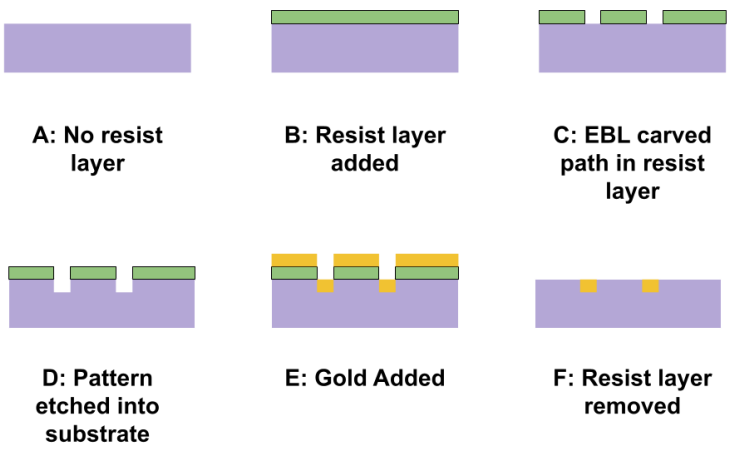

Figure 5:
Each step of the EBL/etching process is shown.

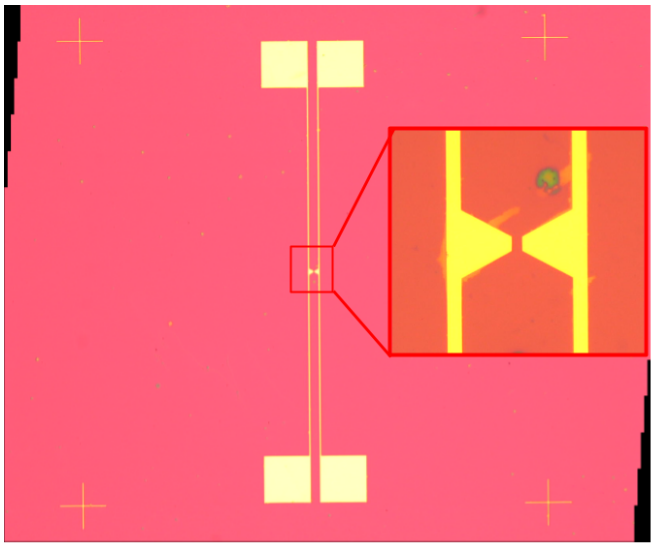

Figure 6:
Full image of antenna pattern before flake transfer with dipole gap enlarged

C. Stamp Preparation

The process of transferring and stacking BP and hBN flakes begins with the creation of *stamps*, which are simple constructions consisting of microscope slides, Polydimethylsiloxane (PDMS), and a polycarbonate (PC) film. The PC film is made first using a PC/Chloroform

solution, which is sandwiched between two glass slides and spread out evenly without bubbles. One slide is removed, and the chloroform evaporates, leaving a thin PC film. Using a tape perimeter, this film can be lifted without tearing.

Preparing the stamp itself involves double-sided tape placed over the end of a slide, as shown in figure 7. A small window is cut in the tape (shown in green) near the edge, and PDMS (orange) is placed in this window. This tape and PDMS is covered by the PC film (red gradient) described above. If done correctly, the film should be clean and uniform, and the stamp can be moved into the glovebox.

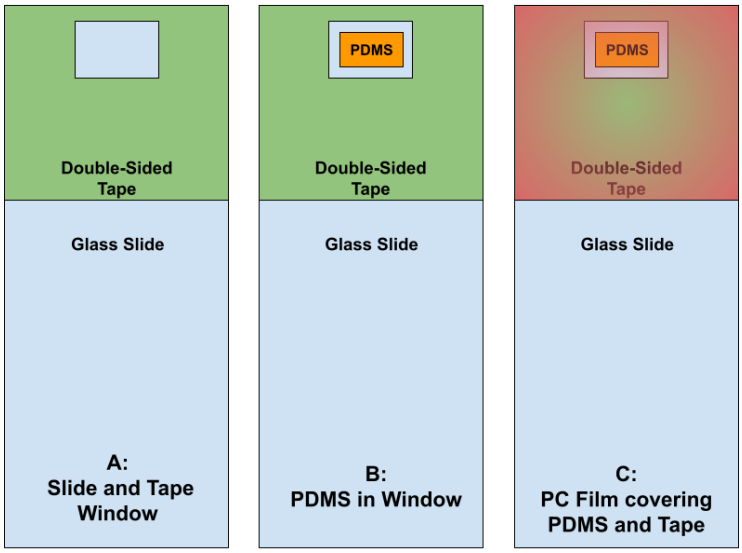

Figure 7:
Three stages of stamp production are shown.

D. Transfers

The process of stacking BP and hBN flakes onto an antenna is not complicated, but it is prone to error. In principle, piezoelectric motors are used to carefully raise an ideal BP flake up and into contact with a stamp, which is oriented PDMS-side-down and fastened securely at a slight tilt. The BP flake and stamp should be aligned such that the flake will come into contact below the PDMS. This process should be done carefully and slowly; even minor bumps are known to tear the PC film, break the stamp's slide, and destroy flakes. In this setup, a microscope helps to visualize when the stamp and flake come into contact, and by using the tilt mentioned above, interference lines will appear shortly before contact. Once in contact, the chip and stamp are heated to 100°C and immediately cooled with a fan. After cooling for an hour, the stamp and chip are slowly separated, and ideally the flake has safely transferred onto the stamp.

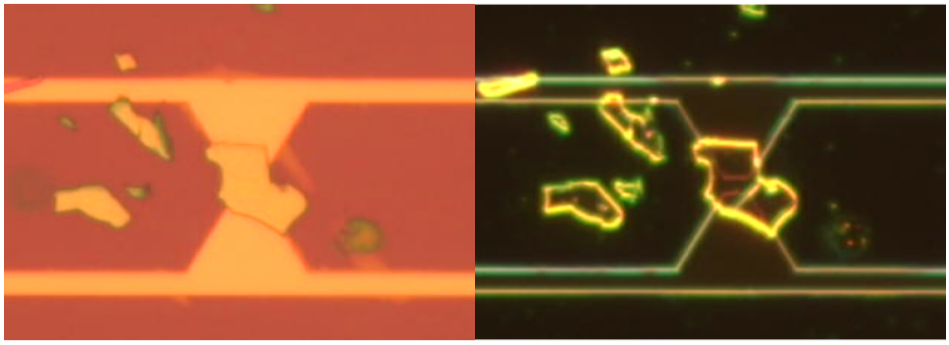

Figure 8:
The black phosphorus flake spans the dipole gap of the antenna. The image on the right was photographed using a darkfield filter.

The next step begins with replacing the exfoliation chip with the antenna chip and then placing the flake onto the antenna, as shown in figure 8. Careful attention is needed to ensure the alignment of the antenna matches the correct orientation of the crystal. After contact is reached following the same steps as before, the stamp and antenna chip are heated to 160°C. Once this temperature is reached the stamp and chip are suddenly pulled apart, which rips the PC film and BP flake from the PDMS, leaving the flake in position on the antenna. Once cooled, the sample is soaked in chloroform for 20 minutes, rinsed in IPA, and finally dried with nitrogen gas. This cleans the sample and removes residue left from the PC film. This same process is used to add an hBN flake to cover the device. This results in a stack where BP is safely guarded against oxygen while still in contact with the antenna, as shown in figure 9. A photograph of the final product is shown in figure 10.

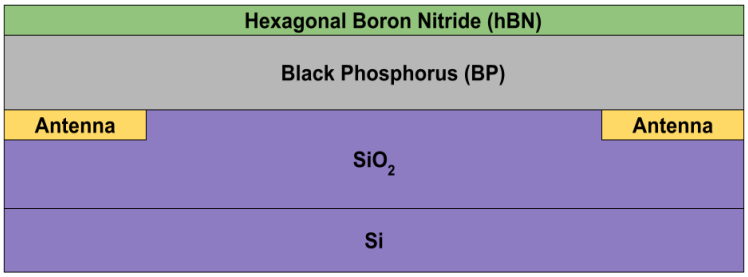

Figure 9:
Stacking schema for THz antenna

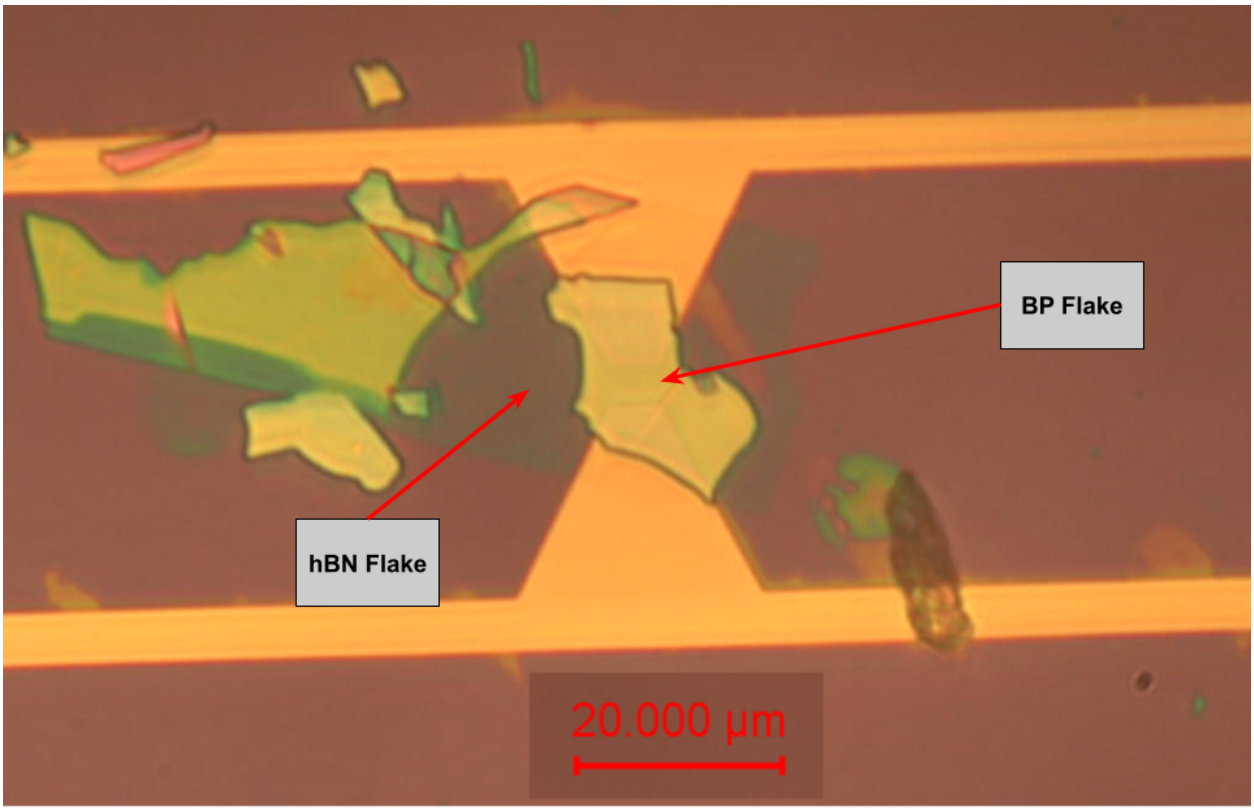

Figure 10:
The Finished Antenna, BP, and hBN stack is shown

E. Device Measurement

A process known as time domain spectroscopy is used to measure the quality of signals produced by this device. In this process, a 780nm laser pulse enters an optical setup and is split along two paths, one of which excites the BP flake. As described above, this creates a terahertz pulse in the antenna, which continues along the first path. The second path, whose pulse can activate a detector, is joined with the terahertz pulse. These beams reach a standard, industrial-grade GaAs terahertz detector, which is activated by the second path's pulse. The detector then takes a 'snapshot' in time of the terahertz signal. The length of the second path can be adjusted, resulting in a measurement at a different point of time. By keeping the first path

constant and varying the path difference, we can obtain hundreds of snapshots of the terahertz pulse, producing a pulse curve as shown in blue in figure 11.

Figure 11:
30V 3mW BP Antenna Signal

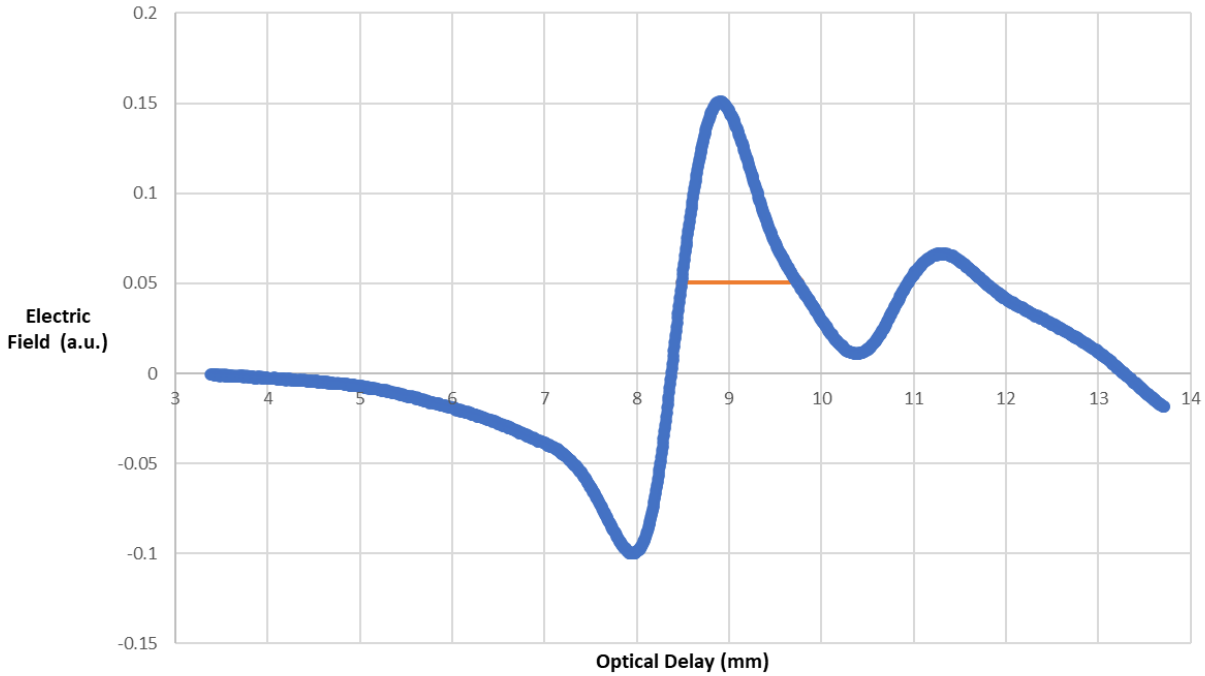

Data

This pulse was produced with a 30V 3mW bias across the dipole gap. Similar measurements were taken at each 5V increment between 5V and 30V. The antenna produced a signal with an electric field amplitude of about A= 0.13a.u., if we define the amplitude as half of the range in the measured electric field values:

$$2A = Max(E) - Min(E)$$

This signal is a pulse rather than a standing wave, so the wavelength and frequency of the signal are not directly measured. To approximate a lower bound on the wavelength, I chose two

points along the main positive peak (domain from 8.5mm to 9.5mm) with y-values approximately a third of the peak's maximum to approximate a pulse width, as shown in orange. This width is calculated as 1.26mm, and by doubling this width I obtain a wavelength of $\lambda = 2.52$mm. Using the wavelength-frequency relation for periodic electromagnetic waves

$$frequency = \frac{c}{\lambda}$$

where c is the speed of light in a vacuum, we obtain an approximate frequency of 0.12THz. These device measurements do not meet the performance expectations given by theoretical considerations [2].

Conclusion

Terahertz-frequency radiation is predicted to have a multitude of practical and scientific applications, including uses in data communications, medicine, and materials science. Devices capable of transmitting and receiving THz signals will require the use of a THz antenna found in many proposed and realized designs. In particular, the BP photoconductive antenna described above shows promising potential as an alternative to standard antennas. The fabrication of this device is straightforward, but it is prone to error and failure. Unfortunately, the presented antenna in particular does not measure up to theoretical expectations and cannot compete with its industry-standard counterparts. However, one particular device is not enough to draw conclusions, and more research is needed.

References

1. Burford, N. M., Evans, M. J., & El-Shenawee, M. O. (2018). Plasmonic nanodisk thin-film terahertz photoconductive antenna. *IEEE Transactions on Terahertz Science and Technology*, *8*(2), 237–247. https://doi.org/10.1109/tthz.2017.2782484
2. Doha, M. H., Santos Batista, J. I., Rawwagah, A. F., Thompson, J. P., Fereidouni, A., Watanabe, K., Taniguchi, T., El-Shenawee, M., & Churchill, H. O. (2020). Integration of multi-layer black phosphorus into photoconductive antennas for thz emission. *Journal of Applied Physics*, *128*(6), 063104. https://doi.org/10.1063/5.0016370
3. He, Y., Chen, Y., Zhang, L., Wong, S.-W., & Chen, Z. N. (2020). An overview of terahertz antennas. *China Communications*, *17*(7), 124–165. https://doi.org/10.23919/j.cc.2020.07.011
4. Mahmoud, S. F., & AlAjmi, A. R. (2012). Characteristics of a new carbon nanotube antenna structure with enhanced radiation in the sub-terahertz range. *IEEE Transactions on Nanotechnology*, *11*(3), 640–646. https://doi.org/10.1109/tnano.2012.2190752
5. Song, H.-J., & Nagatsuma, T. (2011). Present and future of Terahertz Communications. *IEEE Transactions on Terahertz Science and Technology*, *1*(1), 256–263. https://doi.org/10.1109/tthz.2011.2159552
6. Thompson, J., Doha, M., Murphy, P., Hu, J., & Churchill, H. O. H. (2019). Exfoliation and analysis of large-area, air-sensitive two-dimensional materials. *Journal of Visualized Experiments*, (143). https://doi.org/10.3791/58693
7. Welch, K., Doha, M. H., Uttley, Z. P., Fereidouni, A., Omolewu, A., Santos, J., El-Shenawee, M., & Churchill, H. O. (2022). Comparison of hall mobility and carrier density of thin black phosphorus exfoliated from bulk crystals provided by various vendors. *2022 IEEE USNC-URSI Radio Science Meeting (Joint with AP-S Symposium)*. https://doi.org/10.23919/usnc-ursi52669.2022.9887480